J Therm Spray Tech (2021) 30:371–384
https://doi.org/10.1007/s11666-020-01128-0

PEER REVIEWED

Improved Corrosion Protection of Magnesium Alloys AZ31B and AZ91 by Cold-Sprayed Aluminum Coatings

R. P. S. Chakradhar[1] · G. Chandra Mouli[1] · Harish Barshilia[1] · Meenu Srivastava[1]

Submitted: 27 May 2020 / in revised form: 22 October 2020 / Accepted: 12 November 2020 / Published online: 4 January 2021

Abstract Magnesium (Mg) alloys have a high strength/weight ratio, high dimensional stability, good machinability, and the ability to be recycled. However, their poor corrosion resistance in humid environments limits their usage for exterior aerospace components. This study aims to improve the corrosion resistance of two Mg alloys (AZ31B and AZ91) by using aluminum coatings. The latter have been deposited by a low pressure and temperature cold spray process. An aluminum powder (60 wt%) with a particle size ranging between 1 and 8 µm and nickel powder (40 wt%) with a particle size of about 70 µm were blended and used as feedstock powder. The coating thickness was about 240 µm. Its densification was achieved by the in-situ hammering effect of the nickel particles. The shot-peening effect also resulted in an enhanced coating hardness. The microstructure, mechanical properties, and corrosion resistance of the coatings have been investigated. They showed that the aluminum had a face centered cubic structure. Potentiodynamic polarization tests were performed along with a combination of materials characterization techniques to assess the corrosion resistance of the coatings when immersed in a 3.5 wt% NaCl solution for long durations. The results revealed that the corrosion resistance increased with the immersion time because of the formation of a protective oxide layer on the surface. These results were supported by elemental and structural analyses. This study shows that cold-sprayed aluminum coatings are a promising candidate for enhancing the corrosion resistance of AZ31B and AZ91Mg alloys compared to other thermal spray processes.

Keywords Aluminum · Coating · Cold spray · Corrosion · Hardness · Mg alloy

Introduction

In the accelerating expansion of the light metal industry, magnesium (Mg) alloys play an important role in a wide range of engineering applications. The importance of Mg alloys has increased significantly over the years in various industries due to their high strength/weight ratio, high dimensional stability, good machinability, and the ability to be recycled (Ref 1–14). Among the Mg alloys, AZ31B and AZ91 are mostly used for various structural applications in aircraft as well as for the automotive sectors (Ref 2).

Currently, the wrought AZ31B Mg alloy sheet in particular is experiencing increasing attention due to its potential use for thin-walled large-scale components and body structures (Ref 15). Two major drawbacks, however, are poor formability at ambient temperatures and low corrosion resistance in humid saline environments, resulting in galvanic corrosion. Importantly, the corrosion problem currently limits the use of Mg-based aerospace components to about ~ 1 wt% (Ref 16). Mg alloys are predominantly being used in aircraft engine mounts, control hinges, fuel tanks, wings, etc. (Ref 17). Therefore, a thorough understanding of the corrosion behavior of AZ31B and AZ91 Mg alloys could help to increase the corrosion resistance and facilitate expanding their applications in the aerospace sector even to exterior components in order to further reduce the weight.

✉ R. P. S. Chakradhar
chakra@nal.res.in

[1] Surface Engineering Division, CSIR-National Aerospace Laboratories, Bangalore 560017, India

When Mg is exposed to air, it corrodes very quickly. In the past few years, many anti-corrosion techniques have been developed to solve corrosion damage of Mg and its alloys. The common corrosion protection methods considered are microstructure control (Ref 18, 19), composition modification (Ref 20, 21), surface treatments and coatings (Ref 22, 23). In the use of the various wet chemical coatings, the waste water produced during the surface treatment may cause very serious environmental pollution. In practice, cold spraying is a facile and eco–friendly technique used for the corrosion protection of Mg alloys (Ref 24, 25).

Therefore, the main objective of the present work is to develop a corrosion-resistant Al coating for Mg alloys (AZ31B and AZ91) by the low pressure cold spray technique and to study their structural, morphological, and electrochemical properties. Spraying pure Al is challenging as it results in a nozzle clogging phenomenon in which the particles easily stick on the inner surface of the nozzle during the deposition. To overcome the issue of nozzle clogging by the pure Al powder, the first solution consists of reducing the temperature of the nozzle inner wall from the outside by means of cold fluid cooling. Water cooling is an easily affordable solution, and recycled refrigerated CO_2 enables significant efficiency (Ref 26–28). However, the cooling solution cannot prevent another detrimental mechanical interaction between the particles and the nozzle wall which also impacts the longevity of the nozzle (Ref 26). The second solution is to increase the input air pressure in the equipment (DYMET – 423, a low pressure cold spray system). This causes a drop in the nozzle injection pressure thereby decreasing the powder flow in the powder line, hence affecting the quality of the coating. The third solution is to add large-sized metal particles ($\cong$ 70 μm) with a fine Al powder ($<$ 10 μm) to the feedstock, thereby resulting in the free flow of the large-sized particles with pure Al powder from the nozzle to the substrate. This results in a dense coating due to the hammering effect. The use of the hammering effect to obtain dense coatings has been reported by other investigators (Ref 29, 30).

Cold-sprayed Al is expected to greatly reduce corrosion issues in Mg, but more research needs to be carried out to determine the best Al coating. As a corrosion protection coating, Al could serve in two ways, either as a noble barrier coating which shields the substrate from the corrosive environment or as a sacrificial anode which provides cathodic protection for the substrate. However, as a sacrificial anode, there is not much literature available. Further, the significant advantage of using cold-sprayed Al on a Mg alloy component is that the low density of the Mg is retained and the corrosion resistance of the Al is gained. This synergy could be extremely successful in eliminating the galvanic corrosion issues, thereby making Al-coated Mg alloys most suitable for the aerospace and automobile sectors.

Experimental

The starting materials used in the present study are Al powder (99.5% purity; Alfa Aesar) of particle size 1–8 μm and Ni powder (99.9% purity; Metalizing Equipment) of particle size 70 μm. Al powder of 60 wt% was mixed into 40 wt% Ni powder to introduce an enhanced shot-peening effect during the coating process. The mixed powder was mechanically blended for 30 min and then used as the feedstock for the Al coating deposition. The specimens of the AZ31B and AZ91 Mg alloys were cut into dimensions of 40 × 40 × 2 mm^3 and utilized as the substrates for the cold spray. The chemical composition of the base materials in wt% were AZ31B (Al-3.5; Zn-1.3; Mn-1; Si-0.05; Cu-0.05; Fe-0.005; Ca-0.04; Ni-0.005; Mg-balance) and for AZ91 (Al-8.83; Zn-0.62; Mn-0.2; Si-0.01; Cu-0.002; Mg-balance), respectively (Ref 31). The substrates were cleaned in an ultrasonic acetone bath to remove various contaminants by a mechanical scrubbing action. The process involves immersion of the samples in acetone and ultrasonicating them for 10 min. The surface was cleaned from solid dirt, oils, and paints. Thereafter, the substrates were sand-blasted with 200-mesh (70–74 μm) silica using compressed air pressure of 5 bar to create a rough substrate surface.

The particle sizes of the powders were analyzed using a laser particle size analyzer (Malvern). The powder morphology and thickness of the coatings was observed by a field-emission scanning electron microscope (FESEM; Supra 40VP; Carl Zeiss) and an optical microscope. The image analysis was carried out using the image analysis software LAS V4.6 attached to a LEICA MEIREN image analyzer. The composition of the coatings was observed by energy dispersive spectroscopy (EDAX). The 3D roughness profiles were measured using a 3D profilometer (Nano Map 500LS; AEP Technology). Microhardness tests were carried using a Wilson hardness tester (Buehler, USA) as per the ASTM-E-384 standard. The hardness measurements were performed at five different locations and the average values are reported.

An x-ray diffractometry analysis was carried out by a Bruker D8 Advance diffractometer using CuKα (λ = 0.154178 nm) radiation, operated at 40 kV voltage and 40 μA current. The scanning range was 2θ = 30 –90° and the scanning speed was 0.50 min^{-1}. In this study, the Al coating was carried out by using a low-pressure cold spray (LPCS) portable system (DYMET Model–423) with an optimized De Laval nozzle inside a compact spray gun. An axisymmetrical stainless steel nozzle with an exit

diameter of 6 mm, a convergent–divergent spray nozzle with 2.55-mm-diameter throat and a divergent section length of 143 mm was used as the spray gun. The powders were supplied by a vibrational powder feeder connected to the supersonic jet of the nozzle via a radial injection. A number of experiments were carried out by varying the pressure and temperature, and the optimized conditions that resulted in a dense coating were pressure 8 bar, temperature 300° C, and spraying distance of 20 mm. The optimized spraying process parameters are listed in Table 1.

The electrochemical properties of the uncoated and Al-coated AZ31B and AZ91 alloys were comparatively investigated using open-circuit potential (OCP) and potentiodynamic polarization (PDP). These studies were performed using a CH Instruments Electrochemical Work Station (CHI660E). A conventional three-electrode electrochemical cell setup was employed, consisting of the test coupon as the working electrode (sealed by lacquer with an exposed area of 1 cm^2), a platinum electrode as the counter electrode, and a saturated calomel electrode as the reference electrode. All the electrochemical measurements were carried out at different immersion timings in a 3.5 wt% NaCl solution under natural atmospheric conditions. The samples were immersed in corrosive medium (3.5% NaCl, pH 7) at room temperature for about 20 min to establish the open-circuit potential (E_{OCP}). The PDP studies were performed on the sample coupons by applying a cathodic potential drift of -400 mV and an anodic potential drift of +400 mV with respect to E_{OCP} and a scan rate of 1 mVs^{-1}, and a Tafel plot was obtained after the electrochemical measurements. The corrosion potential (E_{corr}), corrosion current density (I_{corr}), and polarization resistance (R_p) were deduced from the Tafel plot (i.e., log I vs. E plot). The I_{corr} values were obtained from the intersect of the Tafel slopes and the R_p values were obtained by using a special analysis tool provided by the Electrochemical work station (CHI660E). After the test, the samples were cleaned with distilled water and ethanol and prepared as per the ASTM standard G31.

Table 1 Process parameters for cold spray coating

Parameters	Values
Carrier gas type	Compressed air
Gas pressure (inside spray gun)	8 bar
Gas temperature (at the input of nozzle)	300° C
Spraying standoff distance	20 mm
Powder feed rate	30 (g/min)

Results and Discussion

Powder Morphology

Figure 1(a) and (b) shows the FESEM images of Al feedstock powder recorded at ×5k and ×10k magnifications, while Fig. 1(c) and (d) shows the optical images of Ni powder recorded at ×50 and ×100, respectively. It can be seen that the morphology of both powders, Al and Ni, are spherical in shape while the Al powder is finer the Ni powder. The particle size distribution obtained from the particle size analyzer for the Al and Ni powders are in the range of 1–8 µm and 40–120 µm, respectively. The Al powder has a mean value $d(0.5)$ of 3 µm, whereas the Ni powder has a mean value $d(0.5)$ of 70 µm.The Ni particles were mechanically mixed into the Al powder to introduce an enhanced hammering effect during the coating deposition process. Assadi et al. (Ref 32) reported that the effective plastic strain governs the density of cold-sprayed metallic coatings. If there exists insufficient plastic deformation of the particles during the particle impact in the coating process, there might be a chance to form inter-particle pores in the coating (Ref 33). In order to obtain dense coating microstructures, the particles should be accelerated to a high velocity to increase the driving force of the particle deformation and/or heating the particles to higher temperature to soften the particles and promote further plastic deformation (Ref 34). In this work, we have adopted the hammering effect, which was achieved by inclusion of the large-sized Ni particles in the feedstock in order to get dense Al coatings on the AZ31B and AZ91 Mg alloys. The Ni content is optimized to obtain a dense Al coating and a critical value of 40 wt% within the mixture was finally selected and used as the feedstock for all the Al coating deposition.

Surface Morphology of the Al Coatings on AZ91 and AZ31 Mg Alloys

Figure 2(a) shows the photograph of the bulk Al coating on AZ91Mg alloy substrate by cold spray. Figure 2(b) and (c) shows the cross-sectional microstructures of the Al coating, whereas Fig. 2(d) shows the splat formation in the coating. During deposition of the coating, the Al particles reveal the plastic deformation and shot peening effect due to the impact of the spherical hard Ni particles. By optimizing the process parameters, it can be clearly seen from Fig. 2(b) that coatings of a thickness as much as ∼ 240 µ m can be achieved by cold spray.

The surface morphology of as-sprayed bulk Al coatings on AZ91 and AZ31B exhibited spherical morphology, as depicted in Fig. 3(a–d) and Fig. 4(a–d) recorded at ×1k,

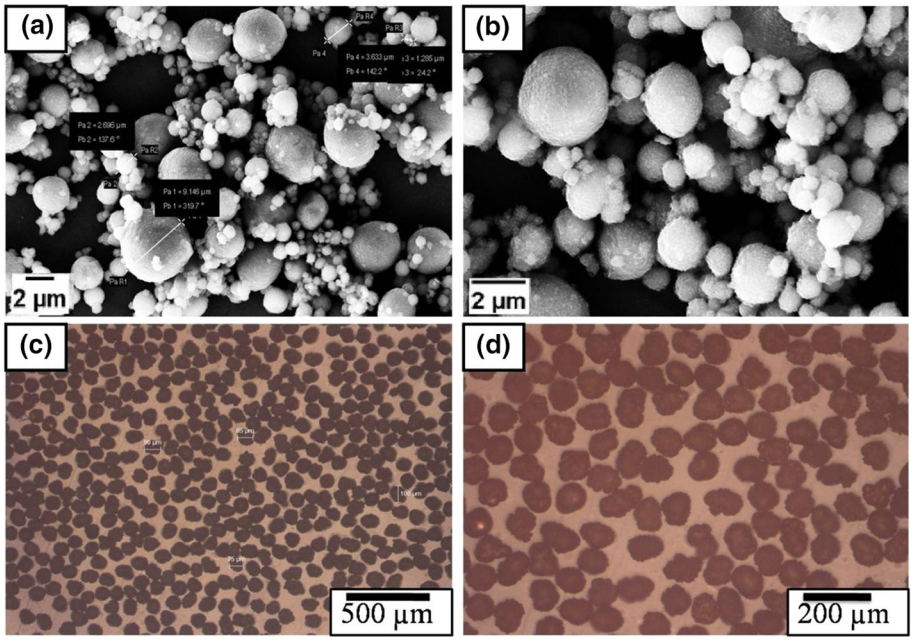

Fig. 1 FESEM images of Al powder (a, b), optical micrographs of Ni powder (c, d)

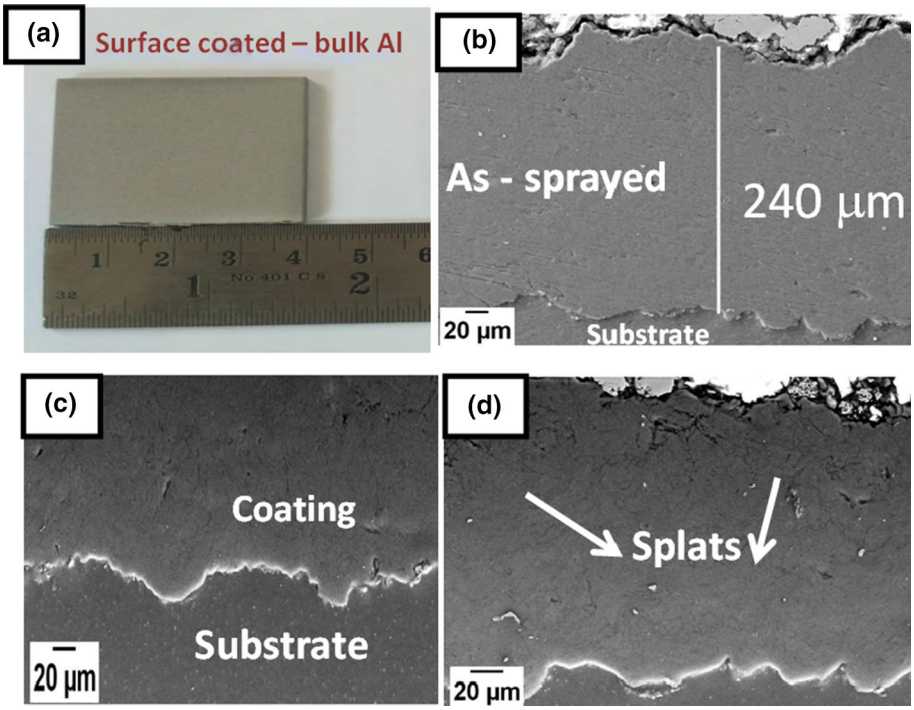

Fig. 2 (a) Bulk Al coating on AZ91, (b, c), close view near the coating/substrate interface, cross-sectional microstructure; (d) Al splat formation in the coating

×2k, ×5k, and ×10k magnifications, respectively. The as-received Al powder shows a spherical morphology and, after coating, the Al powder also retains its spherical morphology and no pores are observed on the surface of the as-sprayed coating. In the coating by large Ni particles, a peening effect is seen in the FESEM images. The surface morphology shows a dense coating which may be due to the fact that the smaller Al particles can be easily accelerated in the supersonic flow, thereby having a larger impact velocity compared to the larger particles (Ref 35). Hence, the coatings produced using the smaller Al particles exhibit low porosity levels compared to the coatings with larger particles under similar conditions.

XRD Studies

Figure 5(a) shows the XRD pattern of the mixed Al and Ni [bulk Al powder (Al 60 wt% + Ni 40 wt%)] feed stock

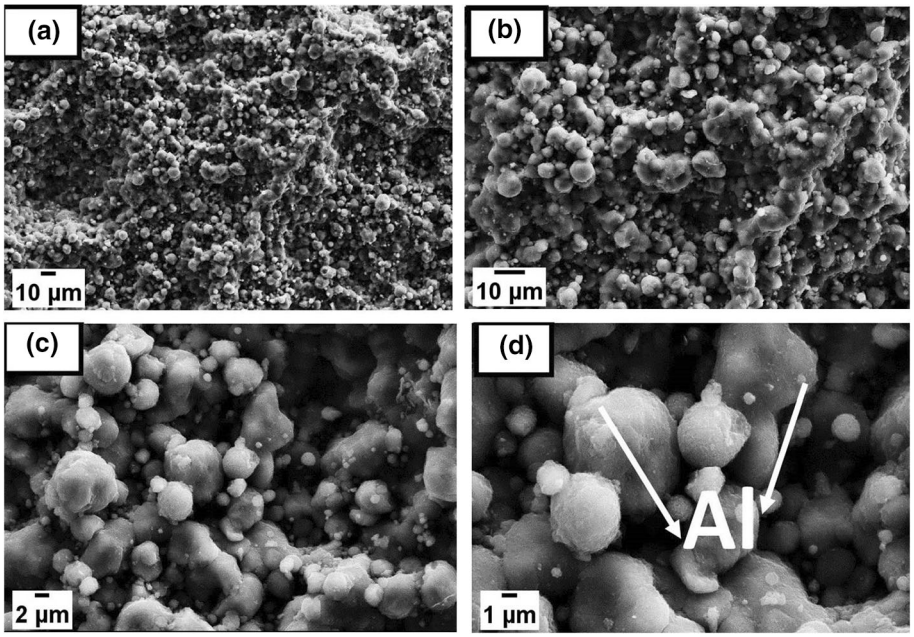

Fig. 3 FESEM images of the as-sprayed bulk Al coating on the AZ91 Mg alloy at different magnifications: (a) ×1k, (b) ×2k, (c) ×5k, and (d) ×10k

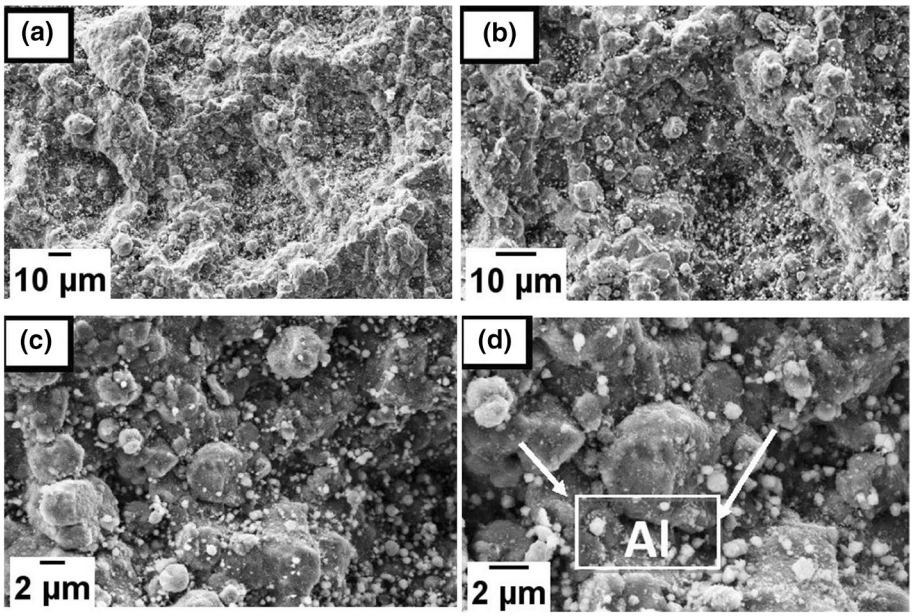

Fig. 4 FESEM images of as-sprayed bulk Al coating on the AZ31B Mg alloy at different magnifications: (a) ×1k, (b) ×2k, (c) ×5k, and (d) ×10k

powder, while Fig. 5(b) and (c) shows the bulk Al coating on the AZ31B and AZ91 Mg alloys, respectively. It can be seen from Fig. 5(a) that the XRD data of the bulk Al powder show the presence of both Al and Ni peaks, which are in agreement with the JCPDS 00-004-0787 and 00-004-0850 data, respectively. The diffraction peaks are indexed and it can be seen that both the Al and Ni powders have a crystal structure of face centered cubic (FCC).

The XRD data of the as-sprayed bulk Al coatings on the AZ31B and AZ91 Mg alloys show the diffraction peaks of just the Al. These peaks were identified and indexed as (111), (200), (220), (311), and (222) lattice planes of the FCC Al structure, perfectly matching the JCPDS 00-004-0787 data of Al. It is interesting to observe that, in comparison with the feed stock powder, the coatings show an absence of Ni peaks, suggesting that pure Al coatings are achieved in this process. The mechanical mixing of Ni particles with the Al powder helped in enhancing the hammering effect during the coating deposition process. Thus, Al coatings of a thickness as much as $\sim$ 240 µm was achieved. The Ni particles significantly contributed to the densification of the coating and then rebounded away during the deposition process. The clogging phenomenon of the Al particles on the inner surface of the nozzle during

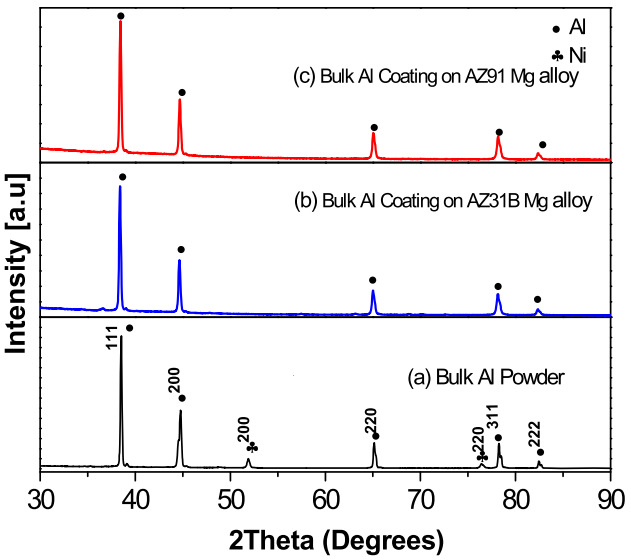

Fig. 5 XRD patterns of (a) feedstock bulk powder and their corresponding as-sprayed Al coating on (b) AZ31B and (c) AZ91 Mg alloys

deposition is also avoided by the mechanical mixing of these larger Ni particles. Further, the absence of new/impurity peaks in the coatings suggest that there is no oxidation or chemical reaction occurring during the coating process. Thus, this confirms that the cold spray process is advantageous compared with other thermal spray processes.

Surface Roughness and Microhardness of the Coatings

The 3D profilometry images of the sand-blasted uncoated AZ31 specimen and the Al-coated AZ31B and AZ 91 Mg alloys are shown in Fig. 6(a), (b) and (c), respectively. It can be seen from Fig. 6(b) and (c) that some mountains and valleys exist in the coating, and the highest average surface roughness, R_a, of 5–6 μm is observed for the Al-coated samples when compared to the sand-blasted sample having a lower average surface roughness of 3 μm, as shown in Fig. 6(a). The coating microhardness is the combined result of high particle deformation upon impact and its related work-hardening (Ref 36). Coatings fabricated from larger particles are harder than those from smaller particles due to the strong peening effect exerted by the higher impact energy of the larger particles (Ref 37). For cold-sprayed composite coatings, the hardness increments of each component from their feedstock states are often different, depending on their degree of plastic deformation (Ref 36). The hardness values of bare AZ31B and AZ91Mg alloys are 70 ± 2 $HV_{0.1}$and 72 ± 2$HV_{0.1}$, respectively. For the bulk Al coatings, the hardness is 78 ± 2 $HV_{0.1}$on the AZ31 Mg alloy, and 80 ± 2 $HV_{0.1}$on the AZ91 alloy. This suggests that the large Ni particles used in the coating for shot peening impact might provide an improvement in the hardness of the coating.

Bu et al. (Ref 35) studied the hardness of commercially pure Al and Al blended with 50 vol% and 75 vol% of the intermetallic $Mg_{17}Al_{12}$ compound coated on the AZ91 Mg alloy by cold spray. The authors observed that, in the case of pure Al, the average hardness was 52 ± 4$HV_{0.1}$ near the substrate interface, and this decreased gradually towards the coating top surface to 43 ± 7$HV_{0.1}$. The authors suggested that the particles near the top surface lack the additional deformation (shot peening effect) provided by the incoming particles, leading to a reduced hardness. The hardness values of the composite coating did not show much difference in comparison with pure Al close to the interface and those at the coating top surface, and the hardness values were reported to be 57.2 ± 2.9$HV_{0.1}$and 59.3 ± 3.1$HV_{0.1}$, respectively. In the present work, an enhanced hardness of the Al coatings is observed (80 ± 2 HV0.1) which is almost twice athat inBu et al. (43 ± 7$HV_{0.1}$) (Ref 35).

Khandanjou et al. (Ref 38) studied the hardness of pure Al coatings at various thicknesses ranging from 150 to 250 μm on a steel substrate deposited by plasma spray. They observed an average value of microhardness in the range 37–40 $HV_{0.25}$. They used a larger particle size of pure Al in the range of 20–75 μm, whereas in the present study a smaller particle size of pure Al in the range 1–8 μm has been used with an enhanced hardness of 80 ± 2 $HV_{0.1}$, which is almost twice what Khandanjou et al. obtained (Ref 38).

Similarly, Fernandez and Jodoin (Ref 39) prepared alumimum–alumina cermet coatings by cold spray. Their studies showed a steady increase in the hardness with the increase in alumina content. However, for the pure Al coating (particle size of 22 μm) without alumina they observed a hardness of 45 ± 8.9 $HV_{0.3}$ which is much lower than the coatings developed in the present study (80 ± 2 $HV_{0.1}$). In order to achieve a higher hardness of ∼ 80 $HV_{0.3}$, Fernandez and Jodoin (Ref 39) used 60% Al_2O_3 in their coatings. When compared to several Al coatings reported by other investigators, the present study has shown a superior hardness for the Al coating. This higher hardness is achieved due to the introduction of an enhanced hammering effect during the coating deposition process as well as by using a reduced particle size of Al (1–8 μm). The reduced particle size as well as an increase in the hammering effect may introduce no or negligible porosity in the coatings, thereby resulting in a higher hardness.

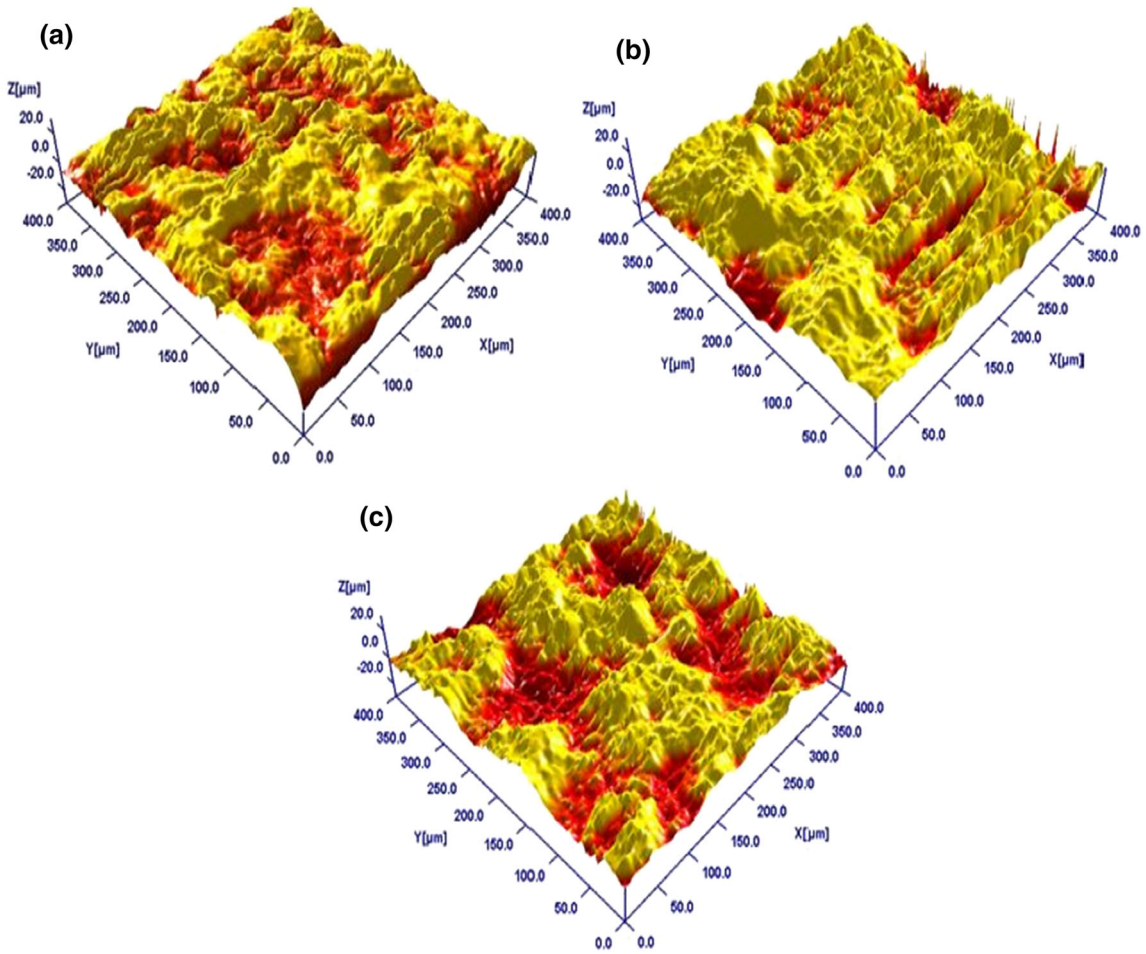

Fig. 6 3D profilometry images of (a) AZ31B sand-blasted (uncoated) sample; Al coatings on (b) AZ31B and (c) AZ91 Mg alloys

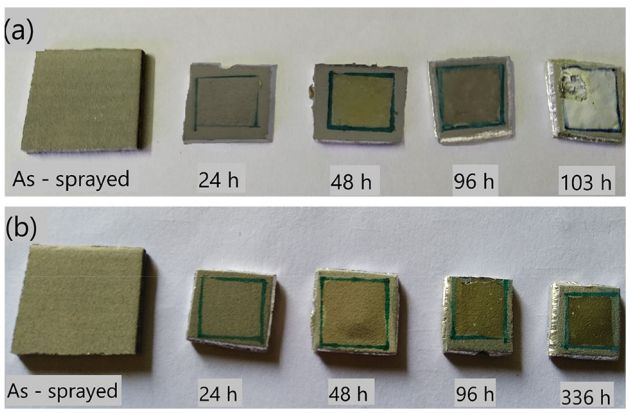

Fig. 7 Bulk Al-coated samples after immersion in NaCl solution as a function of time: (a) AZ31B and (b) AZ91 alloys

Corrosion Behavior of AZ31B and AZ91 Mg Alloys

Visual Appearance of the Surface Exposed to Chloride Medium

Figures 7(a) and (b) shows the photographic images of bulk Al-coated AZ31B and AZ91 alloys after immersion in 3.5% NaCl solution for various durations, 24 h, 48 h, 96 h, and 103 h. The surface of the Al coating on AZ31B and AZ91 appeared as a dark color after immersion for a long time in the NaCl solution. Up to 24 h immersion, there is no change in the appearance of the Al coating, whereas, after 48 h and 96 h, a dark coloration is observed on the surface of the coating. It can be noticed that the Al-coated AZ31B Mg alloy after 96 h of immersion showed no peeling and pit formation. However, after 103 h of immersion, the coating starts peeling which may be attributed to the crack formation on the surface. In the case of the Al-coated AZ91 alloy, after 24 h immersion a dark coloration is observed and thereafter there is no change in the appearance of the Al coating. This appearance

continued for the duration of 336 h and is contrary to the observation of the AZ31B alloy where the coating is peeled-off after 96 h of immersion. This may be associated with the better corrosion resistance of AZ91 compared to AZ31B (Ref 40).

Open Circuit Potential (OCP) Measurements

Figure 8 shows the OCP curves of the Al-coated (a) AZ31B and (b) AZ91 Mg alloys immersed in chloride medium. The OCP of the bare AZ31 alloy is stabilized at −1.60 V after 20 min of immersion. Wei et al. have reported an OCP of −1.47 V for the AZ31B alloy after 1 h of immersion (Ref 41).

The OCP of the cold-sprayed Al-coated Mg alloy is significantly shifted to a positive value of −1.15 V. The positive shift indicates that the coating became more noble due to the oxidation of Al in the medium, resulting in the formation of an oxide film. Increases in the immersion durations to 24, 48, and 96 h resulted in a marginal positive shift in the value to −1.05, −0.98 and −0.81 V, respectively, due to the stabilization of the oxide film.

The OCP of the bare AZ91 alloy is stabilized at −1.60 V after 20 min of immersion, although the value initially shifted in the negative direction and thereafter slowly stabilized. A similar OCP value is reported by Singh et al. for AZ91 alloy (Ref 40). The OCP of the cold-sprayed Al-coated AZ91 Mg alloy shifted to a positive value of −0.98 V. The positive shift indicates that the coating became more noble due to the oxidation of Al in the medium resulting in the formation of an oxide film. An increase in the immersion durations to 24 h and 48 h did not result in a change of the values, i.e., − 0.95 and − 0.94 V, respectively. However, further increases in the duration to 96 h and 336 h resulted in a marginal positive shift in the values to − 0.81 V and − 0.78 V, respectively. The formation of a protective oxide layer is supported by the FESEM, EDAX, and XRD studies and are discussed in detail in subsequent sections.

Potentiodynamic Polarization (PDP) Studies of Al-Coated AZ31B

The PDP curves for the bare AZ31B and cold-sprayed Al-coated alloy are shown in Fig. 9, from which it can be seen that for the bare AZ31B Mg alloy the cathodic reaction is more prominent, i.e., the oxygen reduction reaction taking place as per the following equation:

$$H_2O + 1/2\ O_2 + 2e^- \rightarrow 2OH^-$$

This results in a shift of corrosion potential (− 1.48 V for AZ31B) with respect to OCP (− 1.60 V for AZ31B) due to the change in the pH at the electrode surface. The corrosion potential (E_{corr}), corrosion current density (I_{corr}), and polarization resistance (R_p) have been calculated from the polarization curves and are listed in Table 2.

On the other hand, the Al-coated AZ31B Mg alloy showed a negative shift in potential (−1.22 V as-sprayed coated AZ31B) with respect to OCP (− 1.15 V as-sprayed coated AZ31B). This can be attributed to the oxidation of Al as Al^{3+} and its involvement with the $O\bar{H}$ ions produced by the reduction of water molecules at the cathode. Increases in the immersion duration to 24, 48 and 96 h resulted in a positive shift to −1.20, −1.15 and −0.97 V, respectively, compared to the bulk Al-coated alloy. The positive shift is an indicative of the growth of the oxide film. The corrosion current density, I_{corr}, of the bare AZ31B Mg alloy is ∼ 833.5 μA/cm^2. Wei et al. (Ref 41) reported a current density value of 195.12 μA/cm^2, and the difference is associated with the fact that the samples were ground and polished to a R_a of 0.2 μm prior to testing. However, in the present study, the surface was not subjected to any such treatment. The as-sprayed Al-coated alloy showed a two orders reduction in the I_{corr} value

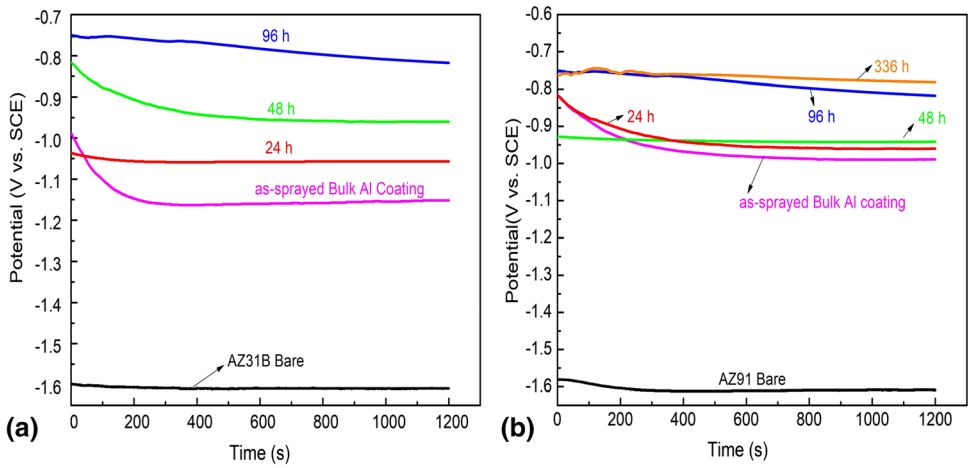

Fig. 8 OCP for bare and Al-coated samples after immersion in NaCl solution as a function of time: (a) AZ31B and (b) AZ91 Mg alloys

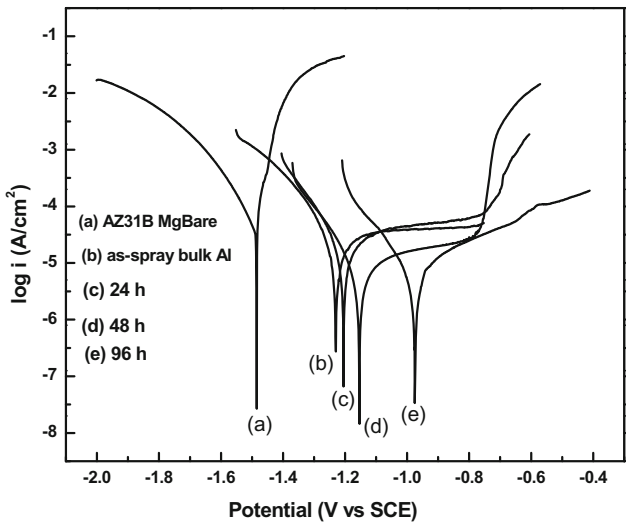

Fig. 9 Polarization curves of (a) bare AZ31B Mg alloy, (b) as-sprayed bulk Al alloy, and the coated alloy immersed for (c) 24 h, (d) 48 h, and (e) 96 h

Table 2 Polarization data of bare AZ31B, as-sprayed bulk Al coatings, and long-term immersion in NaCl for different durations

Samples	E_{corr} (V)	I_{corr} (μA/cm^2)	R_p (Ω cm^2)
Bare AZ31B	−1.48	833.5	777
As-sprayed bulk Al coating	−1.22	5.574	2536
24 h	−1.20	5.465	2835
48 h	−1.15	5.455	2935
96 h	−0.97	4.105	4073

5.574 μA/cm^2, indicating a much slower degradation of Al-coated AZ31B alloy compared to bare (uncoated) AZ31B. The corrosion protection of the cold-sprayed Al coating is marginally better (I_{corr} = 8.88 to 6.01 μA/cm^2) than that of the plasma-sprayed Al coating reported by Khandanjou et al. (Ref 38). Immersion of the Al-coated alloy in 3.5% NaCl medium for 48 h did not result in a change (5.465 μA/cm^2 for 24 h; 5.455 μA/cm^2 for 48 h) in its protection ability. A further increase in the immersion duration to 96 h resulted in a marginal reduction in the corrosion current density to 4.105 μA/cm^2. This indicates that the coated surface is protective in nature. A further increase in the immersion duration resulted in the crack formation and peeling-off of the coating. The polarization resistance, R_p, of the bare AZ31B alloy is 777 Ω cm^2, while covering the surface with a cold-sprayed Al coating resulted in an increase in the value to 2536 Ω cm^2, indicating an improvement in the corrosion resistance of the AZ31B alloy. Immersion of the coated alloy in the chloride medium for 48 h resulted in a marginal enhancement in the value to 2935 Ω cm^2. An increase in the duration to 96 h resulted in a significant increase to 4073 Ω cm^2. This indicates that the corrosion resistance of the coated alloy is retained for 96 h and thereafter it deteriorates.

Characterization of the Coated AZ31B Alloy After Immersion in the Corrosion Medium for 96 h

Figure 10(a–d) shows the surface morphology of the bulk Al-coated surface after 96 h of immersion examined using FESEM at different magnifications. The EDAX analysis of the Al-coated sample after 96 h immersion shows an Al content of 60.40 wt% along with an oxygen content of 39.60 wt%. This suggests the formation of an Al_2O_3 oxide layer which is in an amorphous form. Figure 10(a–c) shows the formation of Al islands, while the EDAX studies confirmed that the dark and white hazy areas relate to aluminum oxide. The formation of this oxide is in accordance with the equations (Ref 42–44):

$$Al^{3+} + 3Cl^{-} \rightarrow AlCl_3$$

$$AlCl_3 + 6H_2O \rightarrow 2Al(OH)_3 + 3HCl$$

The $Al(OH)_3$ gradually converts to $Al_2O_3.2H_2O$, which results in the passivation of the Al surface, which is responsible for the initial constant corrosion current density values for the immersion duration of 48 h. With an increase in the immersion duration to 96 h, the passivation increases, resulting in a further decrease in the corrosion current density values. It is interesting to observe in Fig. 10(d) the formation of a honeycomb-like aluminum oxide structure as a protective layer, which is consistent with the EDAX results.

Figure 11 shows the XRD patterns of the bulk Al coating and the surface after immersion in NaCl solution for different durations of 24 h, 48 h, and 96 h. It can be seen that even after 96 h immersion the coating is intact and the diffraction peaks of Al, are identified and indexed to the (111), (200), (220), (311), and (222) lattice planes of the FCC Al structure that perfectly match with the JCPDS 00-004-0787 data of Al. In addition to the major Al peaks corresponding to the coating, a few minor impurity peaks were detected after 96 h immersion, and are identified as the peaks corresponding to AZ31B. It can be seen that after exposure to a saline environment a protective layer slowly builds up on the Al coating, namely aluminium oxide (Al_2O_3); however, the formation of Al_2O_3 is in an amorphous form. The EDAX results after 96 h immersion show the composition of Al as 60.40 wt% along with an oxygen content of 39.60 wt%, suggesting the formation of an amorphous Al_2O_3 oxide layer. This protective layer is responsible for enhancing the corrosion protection of the Mg alloys that prevent the penetration of chloride ions. The

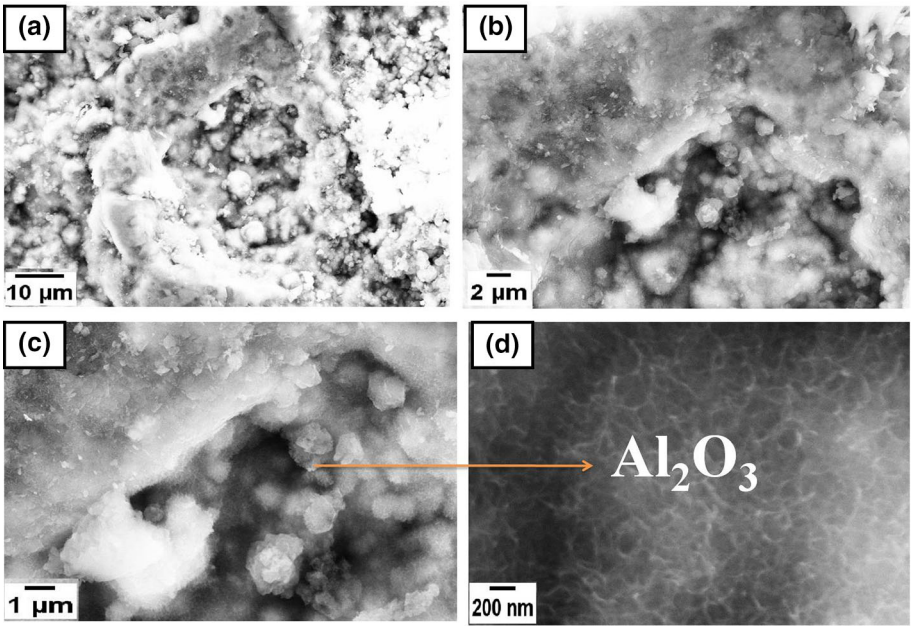

Fig. 10 Surface morphology of the Al-coated AZ31B alloy after immersion in Nacl solution for 96 h at different magnifications: (a) ×2k, (b) ×5k, (c) ×10k, and (d) ×75k

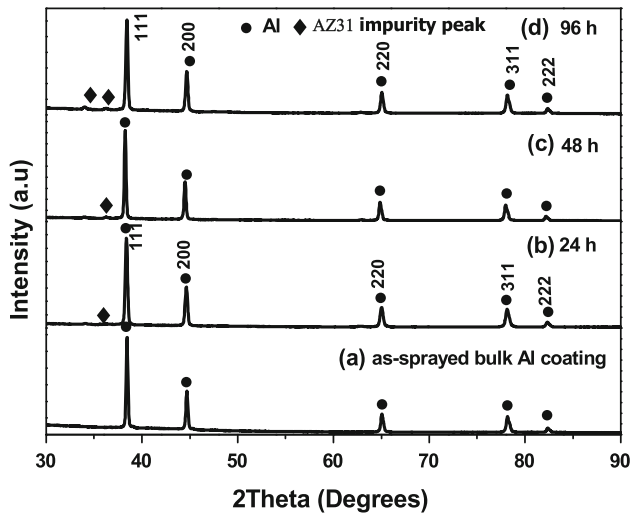

Fig. 11 XRD patterns of (a) the bulk Al coating on AZ31B and the coated surface exposed to: (b) 24 h, (c) 48 h, and (d) 96 h immersion in NaCl solution

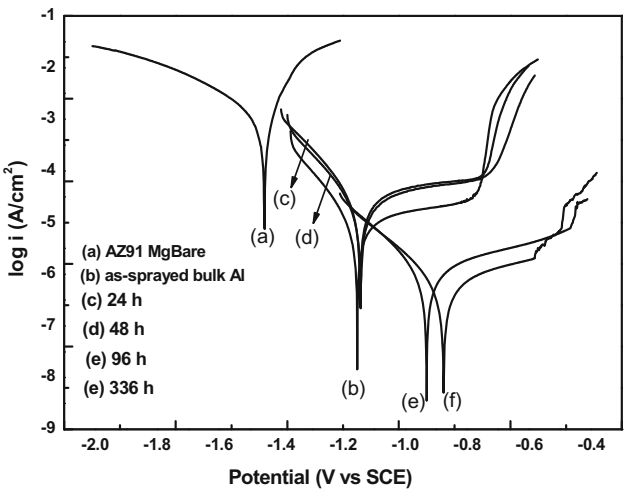

Fig. 12 Polarization plots of bare AZ91, as-sprayed bulk Al-coated alloy, and Al-coated alloy immersed for 24, 48, 96, and 336 h

corresponding change in the morphology of the coatings after immersion is also clearly visualized by the FESEM images.

Potentiodynamic Polarization Studies of Al-coated AZ91

Figure 12 shows the polarization curves obtained for the bare AZ91 alloy and bulk Al-coated alloy for various durations of 24 h, 48 h, 96 h and 336 h, and the obtained polarization data are listed in Table 3. It can be seen that for the bare AZ91 Mg alloy the cathodic reaction is more prominent, similar to the bare AZ31B alloy. Further, from Fig. 12, it can be seen that the anodic polarization curve of

Table 3 Polarization data for the bare AZ91, as-sprayed bulk Al-coated alloy, and Al-coated alloy immersed in NaCl for different durations

Samples	E_{corr} (V)	I_{corr} (μA/cm^2)	R_p (Ω cm^2)
AZ91 bare Mg	−1.45	744.5	1050
As-sprayed bulk Al coating	−1.15	0.5342	4438
24 h	−1.14	0.5016	4639
48 h	−1.14	0.5001	4985
96 h	−0.93	0.3451	8835
336 h	−0.87	0.1236	13,985

the Al-coated alloy exhibits a passive tendency. A similar observation has been made by Bu et al. (Ref 35). The corrosion current density, I_{corr}, for the bare AZ91 alloy is 744.5 μA/cm^2; however, a significant reduction in the value to 0.5342 μA/cm^2 has been observed for the Al-coated alloy.

This indicates that the reactivity of the bare AZ91 Mg alloy is higher in the chloride medium as compared to the cold-sprayed Al-coated alloy, showing that the corrosion resistance of the AZ91 Mg alloy can be significantly enhanced by coating it with a cold-sprayed Al coating. Also, the I_{corr} value of the Al-coated alloy is close to that of the bulk pure Al value of 0.12 μA/cm^2 reported by Bu et al. (Ref 35). Thus, the cold-sprayed Al coating is as dense as the bulk material. Immersion of the Al-coated alloy in 3.5% NaCl resulted in a marginal reduction in the values for a duration up to 48 h. Increases in the duration to 96 and 336 h resulted in a reduction in I_{corr} to 0.3451 and 0.1236 μA/cm^2, respectively.

The corrosion potential of the bare AZ91 alloy, as seen from Table 3, is −1.45 V with respect to OCP (–1.60 V) due to the change in the pH at the electrode surface. Similar corrosion potential values were reported by Bu et al. (Ref 35) and Singh et al. (Ref 40). The I_{corr} value of the cold-sprayed Al-coated AZ91 alloy is −1.15 V, which shows a negative shift in corrosion potential with respect to the OCP (−0.98 V). A similar negative shift was observed in the case of the Al-coated AZ31B alloy, as mentioned in an earlier section. An immersion of the coated alloy in the chloride medium for the long duration of 336 h resulted in a marginal positive shift to –0.87 V. Chunchun et al. (Ref 45) have reported an enhancement in the corrosion protection of sintered NdFeB using a cold-sprayed Al coating. The polarization resistance, R_p, of the bare alloy is 1050 Ω cm^2, while that of the Al-coated alloy has resulted in a significant increase in the value to 4438 Ω cm^2. An increase in the immersion duration to 48 h resulted in a marginal enhancement in the R_p value to 4985 Ω cm^2. A further increase in the immersion duration to 336 h resulted in a significant increase in the value to 13,985 Ω cm^2. This observation is in accordance with the corrosion current density values. The improvement in the corrosion resistance of the Al-coated AZ91 alloy is due to the possible formation of oxides that prevent the penetration of chloride ions.

Characterization of the Coated AZ91 Alloy After Immersion in the Corrosion Medium for 336 h

The formation of a protective film occurs in accordance with the equation discussed earlier. Figure 13 shows the XRD patterns of the bulk Al coating after immersion in NaCl solution for different durations of 24 h, 48 h, 96 h, and 336 h. The diffraction peaks were identified and are indexed to the (111), (200), (220), (311), (222) lattice planes of the FCC Al structure. Small traces of impurity peaks were detected after 336 h immersion, and are identified as the peaks corresponding to AZ91. The surface morphology and elemental composition of the bulk Al-coated AZ91 alloy after 336 h of immersion is displayed in Fig. 14 (a–d) at different magnifications. A nodular morphology is seen on the surface of the specimens. The elemental composition of bulk Al coating after 336 h immersion shows an Al content of 75.40 wt% and oxygen of 24.60 wt%, suggesting the formation of a protective Al_2O_3 oxide layer. The XRD results suggest the formation of a protective oxide layer in an amorphous form which is supported by a significant enhancement in the polarization resistance of the bare alloy from 1050 Ω cm^2 to an Al-coated 13,985 Ω cm^2 even after 336 h immersion. This observation is in accordance with the corrosion current density values. From the above studies, it can be concluded that the cold-sprayed Al coating on the Mg alloys acts as a noble barrier layer, thereby providing enhanced corrosion protection.

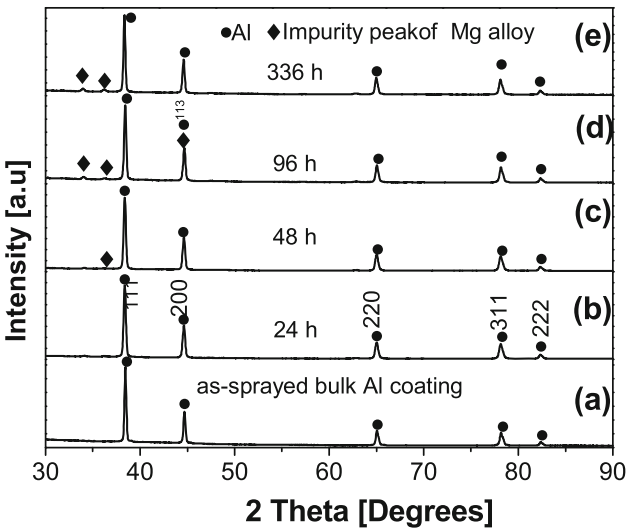

Fig. 13 XRD patterns of (a) the bulk Al coating on AZ91 and the coated surface exposed to (b) 24 h, (c) 48 h, (d) 96 h, and (e) 336 h immersion in NaCl solution

Conclusions

A corrosion protective dense Al coating of ∼ 240 μm thickness has been successfully deposited on AZ31B and AZ91 Mg alloys using a LPCS. The densification mechanism of the coating is achieved by the enhanced in-situ shot-peening and hammering effects. The Al coating exhibits a FCC structure. XRD results show no new/

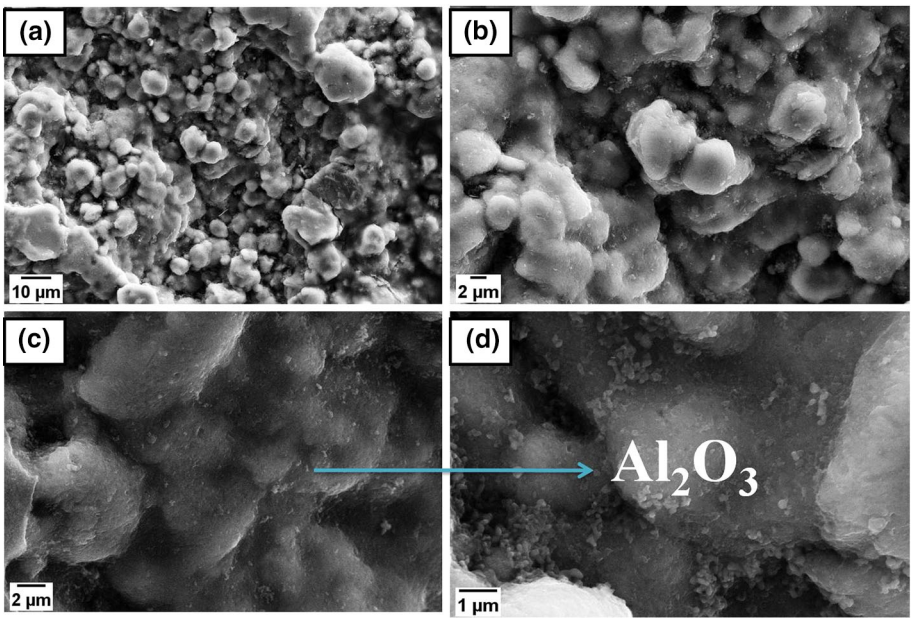

Fig. 14 Surface morphology of the bulk Al coating on the AZ91 alloy after 336 h immersion at different magnifications: (a) ×2k, (b) ×5k, (c) ×10k, and (d) ×25k

impurity peaks in the coatings, which is an indication of there being no oxidation/chemical reactions during the coating process. The coatings showed superior hardness compared to conventional Al coatings due to the hammering effect. The coated samples were subjected to a saline environment for long durations (24, 48, 96, and 336 h) and showed a positive shift in their potential. An increase in the immersion duration to 336 h resulted in a significant increase in the polarization resistance, and this observation is in agreement with the corrosion current density. The experimental results show that the corrosion resistance is enhanced by increasing the immersion time, due to the formation of a protective oxide layer (Al_2O_3) on the surface. These results were supported by XRD, FESEM, and EDAX studies. It can be concluded that the cold-sprayed Al coating on the Mg alloys acts as a noble barrier layer which prevents the penetration of chloride ions, while the coating facilitates an enhanced corrosion protection of the Mg alloys.

Acknowledgements Authors are grateful to the Director, CSIR-National Aerospace Laboratories, Bangalore, for providing the facilities. The authors would like to express their gratitude to Mr. Siju, Mr. Srinivas, and Mr. Praveen Kumar for their assistance rendered during the FESEM, XRD and 3D profilometry characterizations, respectively. The authors would like to thank Dr. M.K. Naidu for his support and encouragement. The present work has not been supported by any funding agency.

References

1. H. Mayer, H.J. Lipowsky, M. Papakyriacou, R. Rosch, A. Stich, and S. Stanzl-Tschegg, Application of Ultrasound for Fatigue Testing of Lightweight Alloys, *Fatigue Fract. Eng. Mater. Struct.*, 1999, **22**, p 591-599. https://doi.org/10.1046/j.1460-2695.1999.00205.x
2. H. Friedrich and S. Schumann, Research for a "New Age of Magnesium" in the Automotive Industry, *J. Mater. Process. Technol.*, 2001, **117**, p 276-281. https://doi.org/10.1016/S0924-0136(01)00780-4
3. G. Davies, *Magnesium: Materials for Automotive Bodies*, Elsevier, London, 2005, p 158-159
4. H. Huo, Y. Li, and F. Wang, Corrosion of AZ91D Magnesium Alloy with a Chemical Conversion Coating and Electroless Nickel Layer, *Corros. Sci.*, 2004, **46**, p 1467-1477. https://doi.org/10.1016/j.corsci.2003.09.023
5. C. Potzies and K.U. Kainer, Fatigue of Magnesium Alloys, *Adv. Eng. Mater.*, 2004, **6**, p 281-289. https://doi.org/10.1002/adem.200400021
6. Z.B. Sajuri, Y. Miyashita, Y. Hosokai, and Y. Mutoh, Effects of Mn Content and Texture On Fatigue Properties of As-Cast and Extruded AZ61 Magnesium Alloys, *Int. J. Mech. Sci.*, 2006, **48**, p 198-209. https://doi.org/10.1016/j.ijmecsci.2005.09.003
7. K. Fritzsch, R. Zenkera, and A. Buchwalder, Improved Surface Properties of AZ31 and AZ91 Mg Alloys Due to Electron Beam Liquid Phase Surface Treatment, *Mater. Today Proc.*, 2015, **2S**, p 188-196. https://doi.org/10.1016/j.matpr.2015.05.009
8. J.X. Li, Y. Zhang, J.Y. Li, and J.X. Xie, Effect of Trace HA on Microstructure, Mechanical Properties and Corrosion Behavior of Mg-2Zn-0.5Sr Alloy, *J. Mater. Sci. Technol.*, 2018, **34**, p 299-310. https://doi.org/10.1016/j.jmst.2017.06.013
9. A. Atrens, S. Johnston, Z. Shi, and M.S. Dargusch, Viewpoint—Understanding Mg Corrosion in the Body for Biodegradable Medical Implants, *Scr. Mater.*, 2018, **154**, p 92-100. https://doi.org/10.1016/j.scriptamat.2018.05.021
10. L.Y. Cui, Y. Hu, R.C. Zeng, Y.X. Yang, D.D. Sun, S.Q. Li, F. Zhang, and E.H. Han, New Insights into the Effect of Tris-HCl and Tris on Corrosion of Magnesium Alloy in Presence of Bicarbonate, Sulfate, Hydrogen Phosphate and Dihydrogen Phosphate Ions, *J. Mater. Sci. Technol.*, 2017, **33**, p 971-988. https://doi.org/10.1016/j.jmst.2017.01.005
11. P. Chakraborty Banerjee, S. Al-Saadi, L. Choudhary, S.E. Harandi, and R. Singh, Magnesium Implants: Prospects and Challenges, *Materials*, 2019, **12**, p 136-157. https://doi.org/10.3390/ma12010136

12. Q. Luo, C. Zhai, Q. Gu, W. Zhu, and Q. Li, Experimental Study and Thermodynamic Evaluation of Mg–La–Zn System, *J. Alloys Compd.*, 2020, **814**, p 152297-152300. https://doi.org/10.1016/j.jallcom.2019.152297
13. W. Wu, Z. Wang, S. Zang, X. Yu, H. Yang, and S. Chang, Research Progress on Surface Treatments of Biodegradable Mg Alloys: A Review, *ACS Omega*, 2020, **5**, p 941-947. https://doi.org/10.1021/acsomega.9b03423
14. H. Somekawa, Effect of Alloying Elements on Fracture Toughness and Ductility in Magnesium Binary Alloys: A Review, *Mater. Trans.*, 2020, **61**, p 1-13. https://doi.org/10.2320/matertrans.MT-M2019185
15. T. Kaneko, M. Suzuhami, Automotive applications of magnesium alloys, in: Y. Kojima, S. Kamado, T. Aizawa, K. Higashi (Eds.) 2nd *Osaka International Conference on PlatformScience and Technology for Advanced Magnesium Alloys, 2003*, pp. 67–74. Trans Tech Publications Ltd, (2003).
16. B. Viehweger, M. During, A. Karabet, and H.J. Hartmann, Evaluation of Forming Behaviour and Tribological Properties of Magnesium Sheet-metal Directly Rolled From Semi-continuously Casted Feedstock, *Magnesium, Proceedings of the 7th International Conference on Magnesium Alloys and Their Applications*, K.-U. Kainer, Ed., Wiley-VCH, Weinheim, 2004, p 377-385
17. N.J. Kim, Critical Assessment 6: Magnesium Sheet Alloys: Viable Alternatives to Steels?, *Mater. Sci. Technol.*, 2014, **30**, p 1925-1928. https://doi.org/10.1179/1743284714y.0000000596
18. Y. Fan, G. Wu, and C. Zhai, Influence of Cerium on the Microstructure, Mechanical Properties and Corrosion Resistance of Magnesium Alloy, *Mater. Sci. Eng., A*, 2006, **433**, p 208-215. https://doi.org/10.1016/j.msea.2006.06.109
19. J. Zhang, J. Xu, W. Cheng, C. Chen, and J. Kang, Corrosion Behavior of Mg–Zn–Y Alloy with Long-period Stacking Ordered Structures, *J. Mater. Sci. Technol.*, 2012, **28**, p 1157-1162. https://doi.org/10.1016/S1005-0302(12)60186-8
20. R. Arrabal, A. Pardo, M.C. Merino, M. Mohedano, P. Casajús, K. Paucar, and G. Garcés, Effect of Nd on the Corrosion Behaviour of AM50 and AZ91D Magnesium Alloys in 3.5 wt% NaCl Solution, *Corros. Sci.*, 2012, **55**(2012), p 301-312. https://doi.org/10.1016/j.corsci.2011.10.033
21. Y. Song, D. Shan, and E.H. Han, Pitting Corrosion of a Rare Earth Mg Alloy GW93, *J. Mater. Sci. Technol.*, 2017, **33**, p 954-960. https://doi.org/10.1016/j.jmst.2017.01.014
22. R.G. Hu, S. Zhang, J.F. Bu, C.J. Lin, and G.L. Song, Recent Progress in Corrosion Protection of Magnesium Alloys by Organic Coatings, *Prog. Org. Coat.*, 2012, **73**, p 129-141. https://doi.org/10.1016/j.porgcoat.2011.10.011
23. W. Liu, Q. Li, and M.C. Li, Corrosion Behaviour Of Hot-Dip Al–Zn–Si and Al–Zn–Si–3 Mg Coatings in NaCl Solution, *Corros. Sci.*, 2017, **121**, p 72-83. https://doi.org/10.1016/j.corsci.2017.03.013
24. A. Viscusi, A. Astarita, R. Della Gatta, and F. Rubino, A Perspective Review on the Bonding Mechanisms in Cold Gas Dynamic Spray, *Surf. Eng.*, 2019, **35**, p 743-771. https://doi.org/10.1080/02670844.2018.1551768
25. W.Y. Li, C.C. Cao, G.Q. Wang, F.F. Wang, Y.X. Xu, and X.W. Yang, Cold spray +' as a New Hybrid Additive Manufacturing Technology: A Literature Review, *Sci. Tech. Weld. Joining.*, 2019, **24**, p 420-445. https://doi.org/10.1080/13621718.2019.1603851
26. R.N. Raoelison, L.L. Koithara, S. Costil, and C. Langlade, Turbulences of the Supersonic Gas Flow During Cold Spraying and Their Negative Effects: A DNS CFD Analysis Coupled with Experimental Observation and Laser Impulse High-Speed Shadowgraphs of the Particles in-Flight Flow, *Int. J. Heat Mass Transf.*, 2020, **147**, p 118894-118913. https://doi.org/10.1016/j.ijheatmasstransfer.2019.118894
27. J. Morère, D. P. Schmidt, P. Liebersbach, J. J. Watkins, Suppression of Clogging in Cold Spray Nozzles, (University of Massachusetts Amherst), CSAT (2018).
28. X. Wang, B. Zhang, J. Lv, and S. Yin, Investigation on the Clogging Behavior and Additional Wall Cooling for the Axial-Injection Cold Spray Nozzle, *J. Therm. Spray Technol.*, 2015, **24**, p 696-701. https://doi.org/10.1007/s11666-015-0227-1
29. Xiao-Tao Luo, Ying-Kang Wei, Yan Wang, and Chang-Jiu Li, Microstructure and Mechanical Property of Ti and Ti6Al4V Prepared by an In Situ Shot Peening Assisted Cold Spraying, *Mater. Des.*, 2015, **85**, p 527-533. https://doi.org/10.1016/j.matdes.2015.07.015
30. Ying-Kang Wei, Xiao-Tao Luo, Cheng-Xin Li, and Chang-Jiu Li, Optimization of In Situ Shot-Peening-Assisted Cold Spraying Parameters for Full Corrosion Protection of Mg alloy by Fully Dense al- Based Alloy Coating, *J. Therm. Spray Technol.*, 2017, **26**, p 173-183. https://doi.org/10.1007/s11666-016-0492-7
31. D. Nakama, K. Katoh, and H. Tokisue, Some Characteristics of AZ31/AZ91 Dissimilar Magnesium Alloy Deposit by Friction Surfacing, *Mater. Trans.*, 2008, **49**, p 1137-1141. https://doi.org/10.2320/matertrans.MC200779
32. H. Assadi, F. Gartner, T. Stoltenhoff, and H. Kreye, Bonding Mechanism in Cold Gas Spraying, *Acta Mater.*, 2003, **51**, p 4379-4394. https://doi.org/10.1016/S1359-6454(03)00274-X
33. S.A. Alidokht, P. Vo, S. Yue, and R.R. Chromik, Cold Spray Deposition of Ni and WC-Reinforced Ni Matrix Composite Coatings, *J. Therm. Spray Technol.*, 2017, **26**, p 1908-1921. https://doi.org/10.1007/s11666-017-0636-4
34. T. Schmidt, F. Gartner, H. Assadi, and H. Kreye, Development of a Generalized Parameter Window for Cold Spray Deposition, *Acta Mater.*, 2006, **54**, p 729-742. https://doi.org/10.1016/j.actamat.2005.10.005
35. H. Bu, M. Yandouzi, C. Lu, D. MacDonald, and B. Jodoin, Cold Spray Blended Al + $Mg_{17}Al_{12}$ Coating for Corrosion Protection of AZ91D Magnesium Alloy, *Surf. Coat. Technol.*, 2012, **207**, p 155-162. https://doi.org/10.1016/j.surfcoat.2012.06.050
36. J. Villafuerte, *Modern Cold Spray: Materials, Process, and Applications*, 1st ed., Springer, Berlin, 2015
37. E. Irissou and B. Arsenault, Investigation of Al-Al_2O_3 Cold Spray Coating Formation and Properties, *J. Thermal Spray Technol.*, 2007, **16**, p 661-668. https://doi.org/10.1007/s11666-007-9086-8
38. S. Khandanjou, M. Ghoranneviss, and S. Saviz, The Detailed Analysis of the Spray Time Effects of the Aluminium Coating Using Self-Generated Atmospheric Plasma Spray System on the Microstructure and Corrosion Behavior, *Results Phys.*, 2017, **7**, p 1440-1445. https://doi.org/10.1016/j.rinp.2017.04.014
39. R. Fernandez and B. Jodoin, Cold Spray Aluminum-Alumina Cermet Coatings: effect of Alumina Content, *J. Thermal Spray Technol.*, 2018, **27**, p 603-623. https://doi.org/10.1007/s11666-018-0702-6
40. I.B. Singh, M. Singh, and S. Das, A comparative corrosion behaviour of Mg, AZ31 and AZ91 alloys in 3.5% NaCl solution, *J. Magnes. Alloys*, 2015, **3**, p 142-148. https://doi.org/10.1016/j.jma.2015.02.004
41. Y.K. Wei, Y.J. Li, Y. Zhang, X.T. Luo, and C.J. Li, Corrosion resistant nickel coating with strong adhesion on AZ31B magnesium alloy prepared by an in situ shot-peening-assisted cold spray, *Corros. Sci.*, 2018, **138**, p 105-115. https://doi.org/10.1016/j.corsci.2018.04.018
42. M. Pourbaix, *Atlas of Electrochemical Equilibria in Aqueous Solutions*, NACE, Houston, 1975
43. R.T. Foley and T.H. Nguyen, Chemical Nature of Aluminum Corrosion—2: the Initial Dissolution Step, *J. Electrochem. Soc.*, 1982, **192**, p 129

44. C.B. Breslin, G. Treacy, and W.M. Cornell, Studies on the Passivation of Aluminium in Chromate and Molybdate Solutions, *Corrosion Sci.*, 1994, **36**, p 1143-1154
45. C. Ma, X. Liu, and C. Zhou, Cold-Sprayed Al Coating for Corrosion Protection of Sintered NdFeB, *J. Thermal Spray Tech.*, 2013, **23**, p 456-462. https://doi.org/10.1007/s11666-013-9994-8